The Journal of Structural Biology
The final publication is available at Elsevier via http://dx.doi.org/10.1016/j.jsb.2016.05.006

Detailed spectroscopic study of the role of Br and Sr in coloured parts of the *Callinectes sapidus* crab claw

M. Katsikini
School of Physics, Aristotle University of Thessaloniki, 54124 Thessaloniki, Greece
E-mail: katsiki@auth.gr; tel: ++30 2310 998500

Abstract
The exoskeleton of crustaceans consists mainly of calcium carbonate ($CaCO_3$) minerals and in many cases exhibits vivid coloration due to the presence of proteins rich in carotenoid chromophores. The exposure of aquatic animals in sea water results often in the incorporation of trace elements in their exoskeleton. The bonding configuration of Br and Sr trace elements in regions with different staining (white, orange and blue) of the exoskeleton of the *Callinectes sapidus* in crab claw are systematically investigated by a number of complementary spectroscopic techniques, including X-ray absorption fine structure spectroscopy (EXAFS), X-ray fluorescence, Raman and visible light reflectivity spectroscopies. It is found that Sr substitutes for Ca and the Sr/Ca ratio is constant along the claw. In the orange region that includes the claw fingers, $CaCO_3$ adopts a calcite-like structure, whereas in the blue and white regions, located in the palm of the claw, an aragonite-like structure dominates. On the other hand, Br, present only in the blue and orange stained parts of the claw, is bound to phenyl and/or phenol rings of amino acid residues, most probably to phenylalanine and/or tyrosine, of the chromophore protein.

Keywords: blue crab, Br, Sr, $CaCO_3$, XAFS, Raman, biominerals

1. Introduction

Hard tissues attract considerable interest due to their excellent mechanical properties attributed to biomineralization which is mainly imposed by the adaptation to a specific biological function. Contrary to vertebrates that possess a bone endoskeleton, crustaceans, like crab, have exoskeleton that stabilizes the body and offers protection from the predators (Hadley, 1986). The exoskeleton comprises of a composite material consisting of α-chitin biopolymers and inorganic minerals, mainly $CaCO_3$ (Nagasawa, 2012). Bone is another example of composite material consisting of hydroxylapatite crystals embedded in a collagen matrix (Wopenka and Pasteris, 2005). Either in bones or in parts of crustaceans' exoskeleton, the formation of biocomposite structures results in materials with outstanding mechanical properties. Variation of the composition, symmetry, size and shape of the $CaCO_3$ biominerals permits control of the mechanical properties of parts of invertebrates' exoskeleton, like jaws, claws, and carapaces. In the case of crabs, the claws are part of the exoskeleton and are used to crack prey and/or to burrow holes (Seed and Hughes, 1995; Zhou *et al.*, 2010).

$CaCO_3$ is abundant in aquatic organisms and is commonly found in three crystalline polymorphs, that is calcite, aragonite and vaterite. However, it has been reported that amorphous calcium carbonate (ACC) exists in a number of different species (Aizenberg *et al.*, 1996; Hasse *et al.*, 2000; Levi-Kalisman *et al.*, 2002; Weiss *et al.*, 2002). Biogenic ACC usually contains significant amounts of Mg and phosphate (Weiner *et al.*, 2003). Its amorphous character is deduced from the absence of well-defined peaks in the X-ray diffraction (XRD) patterns and discrete $CaCO_3$ lattice modes in the low-frequency part of the Raman spectra (Wehrmeister *et al.*, 2011). Rez *et al.* (2014) modelled the X-ray diffraction profiles of biogenic (from plant cystoliths) and synthetic ACC. Their results suggested that randomly oriented 1 nm calcite crystallites were a plausible model. ACC has been proposed as a precursor of crystalline phases like aragonite or calcite (Addadi *et al.*, 2006; Gong *et al.*, 2012; Raz *et al.*, 2010; Weiss *et al.*, 2002). In addition to that, the coexistence of ACC and crystalline phases of $CaCO_3$ has also been reported (Aizenberg *et al.*, 1996; Wehrmeister, *et al.*, 2011; Weiss *et al.*, 2002). Extended X-ray Absorption Fine Structure (EXAFS) spectroscopy is a valuable tool for the detection and study of ACC since its applicability does not depend on the lattice periodicity and has revealed the existence of short-range order that was not otherwise uniquely defined among various organisms (Levi-Kalisman *et al.*, 2002; Weiner *et al.*, 2003). The distinct short-range order that has been observed in various ACC phases is termed as polyamorphism in analogy to the polymorphism that is observed in crystalline $CaCO_3$ (Cartwright *et al.*, 2012). Crystalline phases, aragonite and small amounts of vaterite, were also identified by means of EXAFS (Marxen *et al.*, 2003; Weiss *et al.*, 2002). Since EXAFS is an element-specific non-destructive technique, it is suitable for the study of the bonding configuration of elements incorporated in the exoskeleton either as traces or at larger amounts. Sr is an element that commonly substitutes for Ca in biominerals (Bigi *et al.*, 2007; Brizna et al., 2013; Doubleday *et al.*, 2013; Foster et al., 2009; Lavalli and Spanier, 2007; Tester *et al.*, 2013; Zougrou et al., 2014). Although Sr plays an important role in the nucleation of aragonite *vs*. calcite (Siegel 1960; Sunagawa *et al.*, 2007) and shows a preference for aragonite (Taft, 1967) most probably due to the larger volume that is available, substitution of Ca by Sr in both aragonite and calcite has been reported by Fins and Allison (2007). Crabs, similar to other crustaceans, especially those living in seawater, accumulate Sr with the Sr/Ca ratio being directly related to the concentration of Sr in the environment (Gibbs and Bryan, 1972). Raman spectroscopy has also been applied for the non-

destructive discrimination of crystalline and non-crystalline phases of $CaCO_3$ and for the detection of phosphates (Hasse *et al.*, 2000; Hild *et al.*, 2008; Raz *et al.*, 2000). The position, splitting and Full Width at Half Maximum (FWHM) of the ν_1 stretching mode of CO_3, at *ca.* 1080 cm^{-1}, is a safe fingerprint of the amorphous or crystalline state of $CaCO_3$

Br is another element that is also accumulated by crustaceans. Schofield *et al.* (2009) studied the Br local coordination in the translucent red tips of the claw of the *Pachygrapsus crassipes* crab and correlated the EXAFS results with their mechanical properties. They reported that these tips, which consisted of Br-rich uncalcified tissue that contained about 1% Br, exhibited higher resistance to fracture and hardness compared to the calcified cuticle. Br was found to be bonded to phenyl rings forming bromotyrosine. They attributed the increase in hardness and stiffness to the promotion of Br-induced protein cross-linking and/or to the higher mass of Br. Similar coordination of Br has been also detected in other species (Schofield *et al.*, 2009). In the jaws of the *Nereis* clam worm Br was found to be associated with a variety of amino acids like histidine and tyrosine (Birkedal *et al.*, 2006). Multiple substitutions by Br and other halogens were also reported in the same work.

The blue crab *Callinectes sapidus* is an example of a crustacean that is characterized by the vivid coloration of the exoskeleton (Baldwin and S. Johnsen, 2012). The orange colour of crustaceans, e.g. crab and lobster, has been attributed to astaxanthin (AXT), a keto-carotenoid chromophore. The characteristic colour of carotenoids results from the absorption of light by their long conjugated polyene chain ($\pi \rightarrow \pi^*$ electronic transitions) (Tilley, 2011). In non-aggregated AXT, the $\pi \rightarrow \pi^*$ transition results in absorption that, depending on the polarity of the organic solvent, peaks at 470–490 nm, and is responsible for its orange colour. Aggregation of AXT results in a red-shift of the absorption peak to 390 nm (Buchwald and Jencks, 1968; Cianci *et al.*, 2002; Salares *et al.*, 1977a). AXT is present in the yellow protein of *Homarus americanus* lobster carapace with the absorption spectra exhibiting similar behaviour to aggregated AXT (Cianci *et al.*, 2002). Thus, the shift in the absorption maximum was attributed to chromophore-chromophore excited-state interactions achieved by the aggregation promoted by the yellow protein (Salares *et al.*, 1997a). The distortion of the AXT molecule induced by its binding to the protein was also proposed as a possible mechanism for the shift of the absorption maximum of AXT (Cianci *et al.*, 2002). AXT is also responsible for the blue colour of some crustaceans, when it is non-covalently bound in the crustacyanin protein, where its absorption peak exhibits a strong shift to 580 – 630 nm (Britton *et al.*, 1997; Buchwald and Jencks, 1968; Cianci *et al.*, 2002; Goodwin, 1980; Liu *et al.*, 2002; Salares *et al.*, 1997a; van Wikj, 2005a). One molecule of α-crustacyanin, which is responsible for the colour of the blue lobster, consists of eight β-crustacyanin protein chains each of which binds non-covalently two AXT molecules (Goodwin, 1980). β-crustacyanin is a dimer of type 1 (consisting of A_2 and A_3 apoproteins) and type 2 (consisting of A_1, C_1 and C_2 apoproteins) subunits. The bathochromic shift of the colour of AXT, when bound to crustacyanins, has been attributed to end-ring co-planarization of the polyene chains of AXT and/or to hydrogen bonding of the keto-oxygens of the chromophore molecule that affect the energy gap between the ground and excited states (Cianci *et al.*, 2002; Durbeej and Eriksson, 2003; Salares *et al.*, 1979; Weesie *et al.*, 1995). Variations in the conformation of the AXT molecule and charge transfer (Christensson *et al.*, 2013), stabilization of the enolate form of the AXT molecule (Begum *et al.*, 2015), dimerization of the AXT molecules (Ilagan *et al.*, 2005) and exciton interaction between proximal AXT chromophores (van Wijk *et al.*, 2005b) were also considered as possible mechanisms for the bathochromic shift.

The presence of AXT in the crustacean's exoskeleton can be easily identified by Raman spectroscopy since it provides intense bands at approximately 1500, 1150 and 1000 cm^{-1}.

In this study, EXAFS and Raman spectroscopies are applied for the study of the bonding configuration of Br and Sr along the claw of the *Callinectes sapidus* that exhibits characteristic blue and orange staining alongside with white (unstained) regions. Crustaceans accumulate Br in the form of bromophenols through feeding with algae (Chung *et al.*, 2003). On the other hand, Sr substitutes for Ca and it can be used for the detection of the $CaCO_3$ phases formed along the crab claw providing valuable information on the type of biomineralization. Combination of Raman, visible light reflectivity and X-ray Fluorescence (XRF) spectroscopies establishes a relation between Br and the chromoproteins which are present in the crab exoskeleton.

2. Materials and methods

Different parts of the claw of the *Callinectes sapidus* female crab exhibiting different colouration were investigated by various spectroscopic techniques. Photographs of the claw are shown in Fig. 1(a). The crab was collected in the Thermaikos Gulf, Greece. After removing the soft tissue from the inner part, the claw pieces were cleaned with acetone, methanol and deionised water, they were left to dry and stored in air. The spectra were recorded from pieces from the finger (orange) and the palm (blue and white) of the claw. Reflectivity measurements were conducted using a portable spectrometer (AVANTES) equipped with a Deuterium-Halogen light source and proper optical fibres. The spectra were normalized with the spectrum of a reflecting mirror. The Raman spectra were recorded in the backscattering geometry using a macro-Raman (RAMALOG-5) system equipped with a triple monochromator. Excitation was achieved using the blue-green line (488.0 nm) of an Ar^+ laser and the spectral resolution was approximately 2 cm^{-1}. The incident laser beam was focused on the outer surface of the claw using a spherical lens and the diameter of the spot size on the sample was 1 mm. Monochromator induced shifts were corrected using a Neon calibration lamp. The XRF and XAFS spectra were recorded in air at HASYLAB-DESY at the beamline C of the DORIS ring, using a 7-element Si drift detector positioned on the horizontal plane at right angle to the beam. For the acquisition of the XRF spectra an excitation beam of 16.5 keV was used. The XAFS spectra were recorded at the Sr and Br *K*-edges, at room temperature, by setting proper energy windows to discriminate the Br and Sr K_α emission lines. The incidence angle was 45^o. The EXAFS spectra were analyzed using the ATHENA (Ravel and Newville, 2005), FEFF8 (Rehr and Albers, 2000) and FEFFIT (Newville *et al.*, 1995) programs. The Sr *K*-edge spectra were corrected for self absorption effects taking into account the sample thickness as determined by optical microscopy. For the correction the Booth and Bridges (2005) algorithm was implemented.

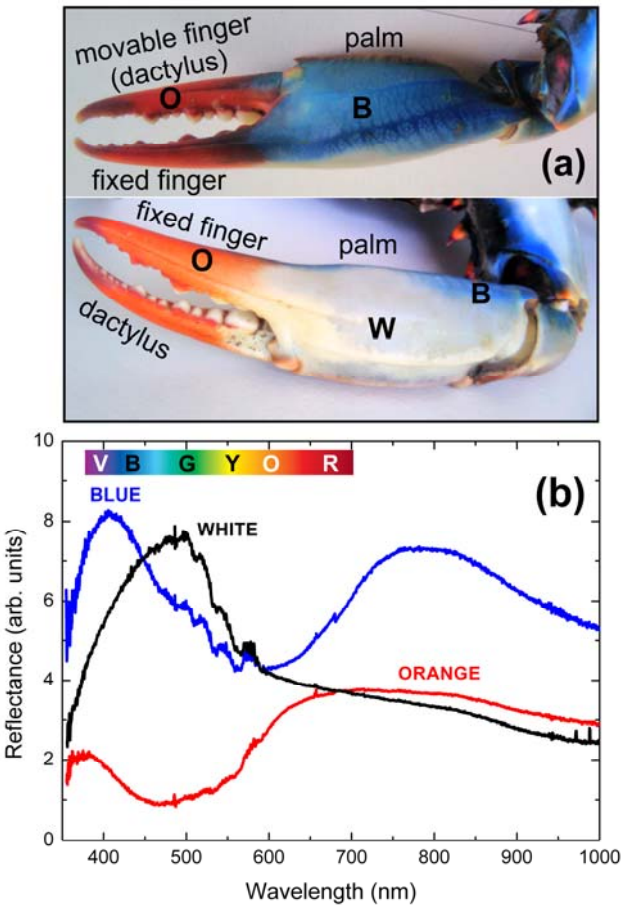

Figure 1: Visible light reflectance spectra recorded from parts of the claw exhibiting different colour. (a) *Photographs of two views of the crab claw. The regions with white, orange and blue colour are labelled with the W, O and B letters, respectively.* ***(b)*** *Visible light reflectance, recorded at 45^o from the white, orange and blue region of the crab claw. The colour bar denotes roughly the wavelength range of the colours of the visible light spectrum, where V, B, G, Y, O and R stand for violet, blue, green, yellow, orange and red, respectively.*

3. Results

3.1. Visible light reflectivity and Raman spectroscopies

The visible light reflectance spectra recorded from regions of the crab claw exhibiting different colour (white, orange and blue) are shown in Fig. 1(b). The shape of the reflectance spectra is directly related to the macroscopic colour of the reflecting object, providing thus valuable information on the structure and composition of the reflecting object. Besides reflection, that occurs on shiny surfaces like that of the crab claw, light propagating in tissues is also attenuated due to various scattering and absorption mechanisms. Assuming that the scattering cross section has smooth frequency dependence, the characteristic blue and orange colour can be ascribed to selective absorption in the spectral regions 500-700 nm and 400-550 nm, respectively. It should be pointed out that in the case of carotenoids, although light absorption from the ground delocalized π-orbital state (S_0) to the excited state (S_2) is strongly electric-dipole allowed resulting in broad absorption bands, fluorescence between these states is a very weak process. This is due to the very rapid relaxation of the molecule *via* non-radiative transitions to a lower-lying excited state (S_1) from which the electronic transition to the ground state is forbidden (Ermakov *et al.*, 2010).

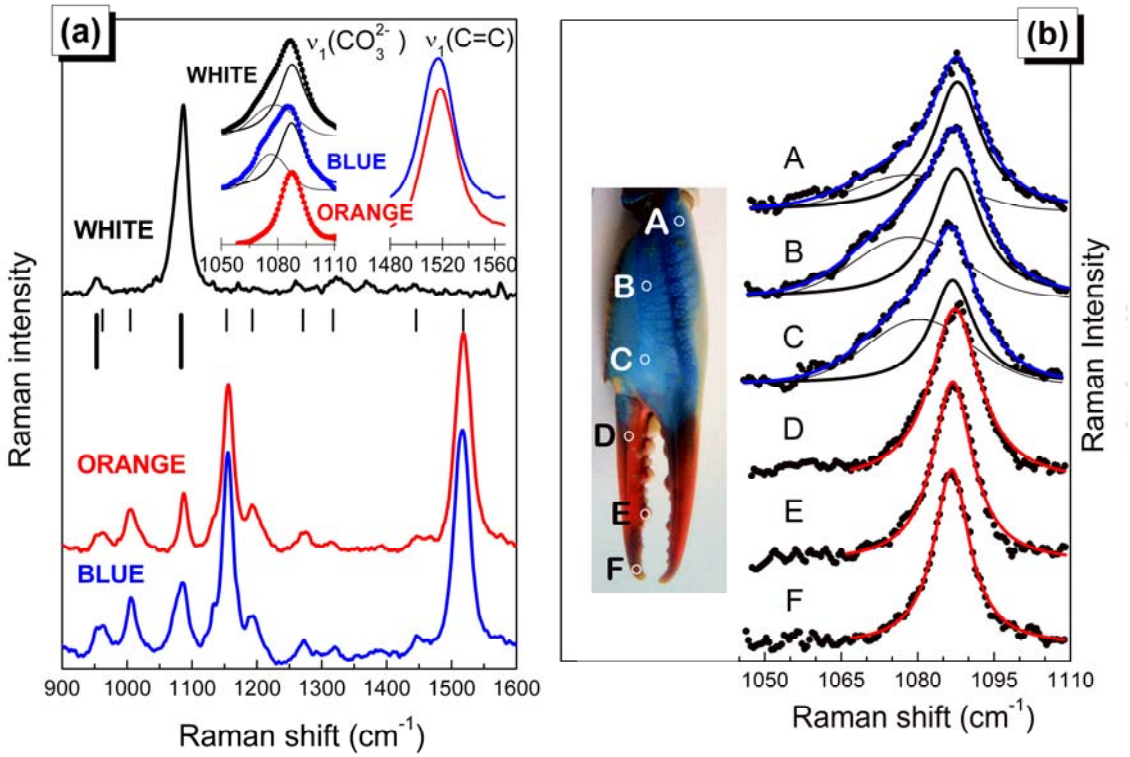

Figure 2: Raman spectra recorded from parts of the claw exhibiting different colour. (a) *Typical Raman spectra recorded in the back-scattering configuration from blue, orange and white regions. Vertical thick and thin lines denote the peak positions assigned to carbonate, phosphate and the astaxanthin chromophore, respectively (see table I). The inset at the top displays a magnification of the spectra around the $\nu_1(CO_3^{2-})$ and ν_1(C=C) peaks along with the fitting of the $\nu_1(CO_3^{2-})$ peak with one Lorentzian (thick line) and one Gaussian (thin line) lineshapes.* ***(b)*** *Raman spectra recorded around the $\nu_1(CO_3)$ peak at various positions along the crab claw which are indicated by A-F marks. The peaks were fitted either with one (Lorentzian) or two (one Lorentzian and one Gaussian) lineshapes shown by thick (1087.0 – 1087.8 cm^{-1}) and thin (1078.3 - 1080.4 cm^{-1}) solid lines, respectively.*

The Raman spectra recorded from the white, orange and blue parts of the crab claw are shown in Fig. 2(a). The Raman shifts of the detected peaks are in agreement with published data and are listed in Table I along with their assignments (Kaczor and Baranska, 2011; Penel *et al.*, 1998; Salares *et al.*, 1977a; Weesie *et al.*, 1999). The Raman spectrum recorded from the white region differs considerably from the spectra obtained from the stained parts of the claw. The spectrum of the white region is dominated by two well defined peaks originating from the carbonate (CO_3^{2-}) and the phosphate (PO_4^{3-}) anions at 1083 and 952 cm^{-1}, respectively (Penel *et al.*, 1998). The relative integrated area under the phosphate to carbonate peaks is 1:30. The carbonate peak originates from the $CaCO_3$ biomineral present in the crab exoskeleton and exhibits considerable broadening implying the presence of $CaCO_3$ nanocrystallites or even of ACC $CaCO_3$ phases of low crystallinity. Indeed, a closer view of the peak reveals an asymmetry towards lower wavenumbers, which can be successfully reproduced by introducing two lineshapes in the fitting, one Lorentzian and one Gaussian. The decomposition of the carbonate peak in two lineshapes is shown in the inset of Fig. 2(a). The two peaks are located at 1078 and 1087 cm^{-1} and the corresponding FWHMs are

26 and 18 cm^{-1}, respectively. Similarly, Wehrmeister *et al.* (2011) used two lineshapes, one Lorentzian and one Gaussian, to account for the presence of a crystalline and an amorphous phase. They assigned the $\nu_1(CO_3)$ peak located at 1078 cm^{-1} to an ACC phase and the peak at 1087 cm^{-1} to a crystalline phase, calcite or aragonite (Behrens *et al.*, 1995). Therefore, the results on the *C. sapidus* studied here, indicate the presence of two $CaCO_3$ phases. The one that is termed as crystalline is rather nano-crystalline as it can be deduced from the FWHM of the corresponding peak that is 4 times higher than the FWHM of a crystalline calcite reference (4.4 cm^{-1}). The second is termed as amorphous due to the much broader character of the assigned peak and its shift towards lower frequencies. The mode softening and the high FWHM are induced by the structural disorder that causes relaxation or breakdown of the selection rules. It should be pointed out that the position of the $\nu_1(CO_3)$ peak can not be directly used for the discrimination of the calcite or aragonite phase (Wehrmeister *et al.*, 2011).

Table I: Analysis results of Raman spectra. *Raman peaks' energy position and FWHM (in parentheses) obtained by using appropriate lineshape fitting (see text) for spectra recorded from regions of the crab claw with different colours. Assignment of the corresponding vibrational modes based on the literature is also provided.*

Peak position (cm^{-1})			
White area	**Orange area**	**Blue area**	Assignment*
953	952	952	ν_1 (PO_4^{-3})
-	964	964	*AXT*: C-H out of plane bending
-	1007	1005	*AXT*: CH_3 rocking (ν_3)
1078 (26) 1087 (18)	1088 (15)	1076 (20) 1087 (17)	*CaCO3*: ν_1 (CO_3^{2-})
-	1156	1156	*AXT*: mixed C-C stretching and C-H in plane bending (ν_2)
-	1195	1193	*AXT*
-	1273	1272	*AXT*: C-H in plane bending
-	1312	1318	
-	1448	1446	
-	1518	1516	*AXT*: C=C stretching (ν_1)

* Kaczor and Baranska, 2011; Penel *et al.*, 1998 ; Salares *et al.*, 1977a; Weesie *et al.*, 1999

The crystallinity index, defined as the relative areas of the nanocrystalline to amorphous phase (Wehrmeister *et al.*, 2011), is found equal to 2.3 (i.e. 30% amorphous phase). The peaks due to CO_3^{2-} and PO_4^{3-} are also present in the Raman spectra recorded from the blue and orange regions. The CO_3^{2-} peak still exhibits a low energy asymmetry in the blue region with the same crystallinity index as the white one. In contrast, in the spectrum recorded from the orange region of the claw only one carbonate contribution, at 1088 cm^{-1}, is detected with a definitively lower FWHM of 15 cm^{-1}. Since the orange region includes the claw fingers, the results convincingly suggest a different type of $CaCO_3$ biomineralization at the end of the claw. The presence of vaterite in the blue and

white regions of the claw should not be excluded. In vaterite, the $\nu_1(CO_3)$ mode is decomposed to three peaks, at 1075, 1081, 1091 cm^{-1} (Wehrmeister *et al.*, 2011), and could account, after significant broadening due the nano-crystalline character of the $CaCO_3$ phase, for the asymmetric $\nu_1(CO_3)$ peak (Behrens *et al.*, 1995). Such decomposition was not possible due the broad character of the peak. It should be noted that the Raman spectra recorded from the palm at lower wavenumbers, i.e. where the lattice modes of $CaCO_3$ are expected, were featureless. In the spectrum recorded from the finger, a very weak broad peak centred at 287 cm^{-1} is observed i.e. close to the a lattice mode of calcite (Behrens *et al.*, 1995).

To reveal any position-dependent variation in the $\nu_1(CO_3)$ peak lineshape, Raman spectra were recorded at various spots along the claw. The spectra shown in Fig. 2(b) clearly reveal that the $\nu_1(CO_3)$ peak has only one contribution, at 1086.7 to 1087.3±0.1 cm^{-1}, in the spectra recorded from the finger. The FWHM of the Lorentzian used to fit the corresponding peak in the spectra recorded from points E (tooth) and F (finger tip) is even smaller (8.8 and 8.1±0.3 cm^{-1}, respectively) compared to FWHM of the peak in the spectrum recorded from point D. Contrary to the spectra recorded from the claw finger, the $\nu_1(CO_3)$ peak in the spectra recoded from the palm has two contributions fitted with one Lorentzian (1087.0-1087.8 ±0.1 cm^{-1}) and one Gaussian (1079 ±2 cm^{-1}) lineshape. The crystallinity index defined above, is found equal to 2.5±1, 1.5±0.3 and 1.0±0.2 at the A, B, and C spots, respectively.

The general overview of the Raman spectra recorded from the blue and orange regions of the claw is considerably different from that recorded from the white region. More specifically, additional bands appear in the frequency regions 1000, 1150 and 1500 cm^{-1} which are characteristic of the presence of carotenoid chromophores (Weesie *et al.*, 1999). The most intense peak (ν_1) located at 1515 cm^{-1} has been assigned to the C=C bond stretching. Its frequency value depends on the degree of conjugation and length of the polyene chain of the carotenoid molecule, the polarization induced by polar solvents and the planarity of the chain (Rimai *et al.*, 1973; Salares *et al.*, 1977a, 1977b; Weesie *et al.*, 1995). The second most intense peak at *ca.* 1150 cm^{-1} (ν_2) has contributions from both C-C stretching of the polyene chain and in-plane C-H bending whereas the third, at approximately 1005 cm^{-1} (ν_3), corresponds to CH_3 rocking vibrations. Assignment of the less strong peaks is also included in Table I. The Raman spectra strongly suggest the presence of a carotenoid chromophore, presumably AXT, in both the orange and blue regions. The relative constancy of the chromophore Raman peaks intensities indicate also a corresponding immutability of AXT in the stained regions. Regarding the positions of the main AXT peaks, the ν_1 and ν_3 appear red-shifted by 2 cm^{-1} in the spectrum recorded from the blue region compared to that recorded from the orange part of the claw, whereas the ν_2 peak remains unshifted. Such behaviour has also been reported by Salares *et al.* (1977a) and has been attributed to resonance effects in the Raman spectra.

3.2. XRF and XAFS spectroscopy

Typical XRF spectra recorded from regions with different colour are shown in Fig. 3. Irrespective of the colour, the emission peaks due to Ca [3.7 (K_α) and 4.0 keV (K_β)] and Sr [14.1 (K_α) and 15.8 keV (K_β)] are detected. The Sr/Ca atomic ratio was estimated from the intergraded areas ratio under the corresponding K_α emission peaks, I_{Sr} and I_{Ca} in the XRF spectra using the equation:

$$\frac{Sr}{Ca} = \frac{I_{Sr}}{I_{Ca}} \frac{\omega_{Ca} g_{Ca} (\mu/\rho)_{Ca,E_0} (1 - 1/J_{Ca})}{\omega_{Sr} g_{Sr} (\mu/\rho)_{Sr,E_0} (1 - 1/J_{Sr})} \quad (1)$$

where ω_i, g_i, J_i, and $(\mu/\rho)_{I,Eo}$, for i=Ca, Sr, are the fluorescence yields of the *K* shell, the emission probability of the K_α line from the K series, the jump ratio for the K edge and the photoabsorption cross section for the *K* shell and for excitation energy E_0, respectively (Janssens *et al.*, 2000; Katsikini *et al.*, 2010). Since the XRF spectra were recorded in air, the intensity of the Ca K_α emission line was corrected for the sample to detector air-path absorption using the law of Beer-Lambert and the air's absorption coefficient.

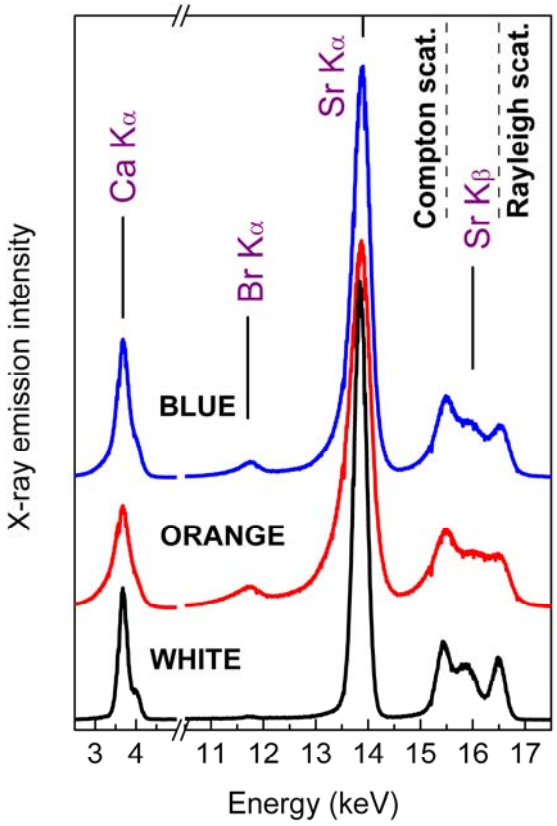

Figure 3: XRF spectra recorded from parts of the claw exhibiting different colour. *Representative XRF spectra recorded from areas of the claw with different colouration. The excitation energy was 16.5 keV. The energy positions of the K emission lines of Ca, Br and Sr as well as those of the elastic (Rayleigh) and inelastic (Compton) scattering peaks are indicated with vertical lines.*

The Sr/Ca atomic ratio was found to be equal to 0.055±0.003 and did not exhibit variations in the regions with different colour. Nevertheless, as it can be deduced from the corresponding low-intensity emission line in the XRF spectra shown in Fig. 3, small amounts of Br are present in the stained regions of the crab claw. The Br/Ca weight ratio determined using the Eq. 1 is found equal to 0.60 ±0.05 mg/gr. The corresponding atomic ratio is $(0.27\pm0.02)\times10^{-3}$. The fact that both Br and AXT are detected (using XRF and Raman spectroscopies, respectively) in the stained claw regions indicates that Br is most probably trapped in the chromophore-protein. Furthermore, since staining is present only in a thin surface layer of the exoskeleton, the Br/Ca ratio is directly affected by the thickness of this layer.

In order to identify the Br- and Sr- bonding configuration in the crab claw shell, XAFS measurements were conducted at the Br and Sr *K*-edges from claw regions with different colour. The Br *K*-edge XANES and EXAFS spectra recorded from the orange- and blue-stained claw regions are shown in Fig. 4.

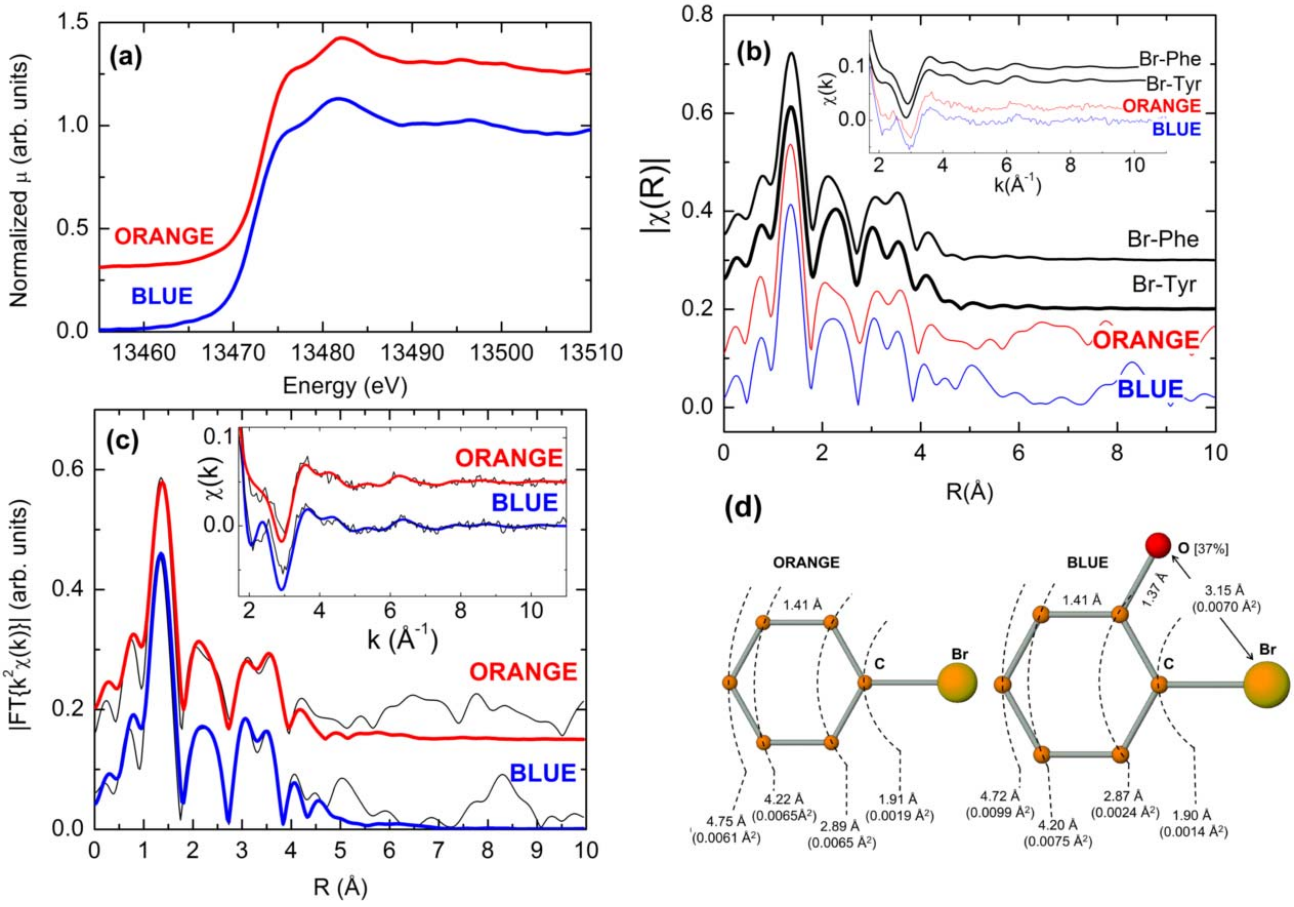

Figure 4: Br K-edge XAFS spectra. *Representative Br K-edge XAFS spectra recorded from the orange and blue regions:* ***(a)*** *XANES spectra (vertically shifted for clarity);* ***(b)*** *Simulation of the EXAFS spectra in R- and k-(shown in the inset) space using models of Br bonded to a phenyl ring as in bromo-phenylalanine (Br-Phe) and of Br bonded to a phenol ring as in bromo-tyrosine (Br-Tyr). The Equation of Motion routine of FEFF was utilized for the estimation of the Debye-Waller factors of single and multiple scattering paths.* ***(c)*** *Fitting of the EXAFS spectra in R- and k- (shown in the inset) space. The experimental spectra and the fitting curves are indicated by thin and thick solid lines, respectively;* ***(d)*** *Schematic representation of the fitting results.*

The Br *K*-edge XANES spectra shown in Fig. 4(a) have similar characteristics with the spectra from reference compounds where one or two Br atoms are bonded to a benzene ring (Feiters *et al.*, 2005a). The strong contributions up to the distance of *ca.* 6 Å in the Fourier Transform (R-space) of the χ(k)-EXAFS spectra shown in Fig. 4(b) are characteristic of strong multiple scattering, and has also been observed in other cases of Br bonded with benzene rings (Bergknut *et al.*, 2008; Feiters *et al.*, 2005a; Schofield *et al.*, 2009). In order to decide on the optimum model for the fitting, the EXAFS spectra were simulated using two models denoted as Br-Phe and Br-Tyr. In the former the Br atom is bonded to a phenyl (benzene) ring whereas in the latter it is bonded to a phenol ring, as

described in the Supporting Information file. These models account for bonding of Br to the aromatic amino acids phenylalanine/tryptophan and tyrosine, respectively. The Debye-Waller factors of the single and multiple scattering paths were calculated using the Equation of Motion routine that is incorporated in the FEFF8 code (Poiarkova and Rehr, 1999). The simulated spectra are compared with the experimental spectra in the k- and R-space in Fig. 4(b). Both models reproduce very well the spectral features, with the Br-Tyr model being more appropriate for the case of the spectrum recorded from the blue part of the claw. A representative fitting of the Br *K*-edge EXAFS spectra in the R- and k-space is shown in Fig. 4(c). The fitting was performed using single- and multiple-scattering photoelectron paths obtained by FEFF8 using the Br-Phe and Br-Tyr models for the spectra recoded from the orange and the blue parts of the claw, respectively, as shown schematically in Fig. 4(d). The scattering potentials were calculated self-consistently using a Hedin-Lundqvist self-energy (Rehr and Albers, 2000). Details on the analysis procedure and the paths used for the fitting can be found in the Supporting Information file. The Br-Phe model provided very good fitting quality in the case of the spectrum recorded from the orange part of the claw and the inclusion of O-related paths was not necessary. In the case of the spectrum recorded from the blue part of the claw, the coordination numbers of the O- related single and multiple scattering paths were weighted by a factor x to account for Br bonding to both phenyl and phenol rings. The fitting procedure provided a value of x equal to 0.37±0.2 revealing that Br is bonded to both phenyl and phenol rings. Therefore, the results suggest that Br is bonded to aromatic rings of aromatic amino-acids. The nearest neighbour distances, as determined from the fitting and the corresponding Debye-Waller factors (in parentheses) are also shown in Fig. 4(d) for single scattering paths. The C-C distance was determined from the proper combination of the single scattering paths used to construct the multiple scattering ones.

The XANES and the EXAFS spectra recorded at the Sr *K*-edge are shown in Fig. 5. The XANES spectrum, Fig. 5(a), recorded from the orange region exhibits differences compared to the spectra recorded from the white and blue regions, revealing variations in the bonding configuration of the Sr atoms. Differences are also observed in the EXAFS spectra, shown in Fig. 5(b), which were recorded from the orange and blue/white regions. The EXAFS spectra were fitted using the calcite model assuming that the central, absorbing, Ca atom was replaced by a Sr atom. The fitting of the EXAFS spectra, both in the R- and k-space, are shown in Fig. 5(b) whereas the results are summarized in Table II. For the sake of completeness, the bonding configuration of Ca in calcite and aragonite ($CaCO_3$) and Sr in strontianite ($SrCO_3$) model compounds is also included in Table II (de Villiers, 1971; Graf, 1961). The results show conclusively that in the orange region of the claw (fingers), Sr participates in the formation of a different phase. The Sr-O distance is found equal to 2.53 Å in the orange and 2.60-2.62 Å in the blue and white regions. Since variations in the Sr/Ca ratio are not observed along the claw, the shorter distance could be attributed to the formation of a calcite-like phase in consistence with the fitting results for shells at larger distances. Spectra recorded from the palm of the claw, exhibiting blue and white coloration, suggest that the aragonite phase dominates. It should be noted that the vaterite model did not yield good quality fitting of the spectra recorded from both the palm and the fingers of the claw. In all cases the large values of the Debye-Waller factors indicate the formation of poorly-crystallized phases, a finding that is in line with the considerably high degree of static disorder detected by Raman spectroscopy.

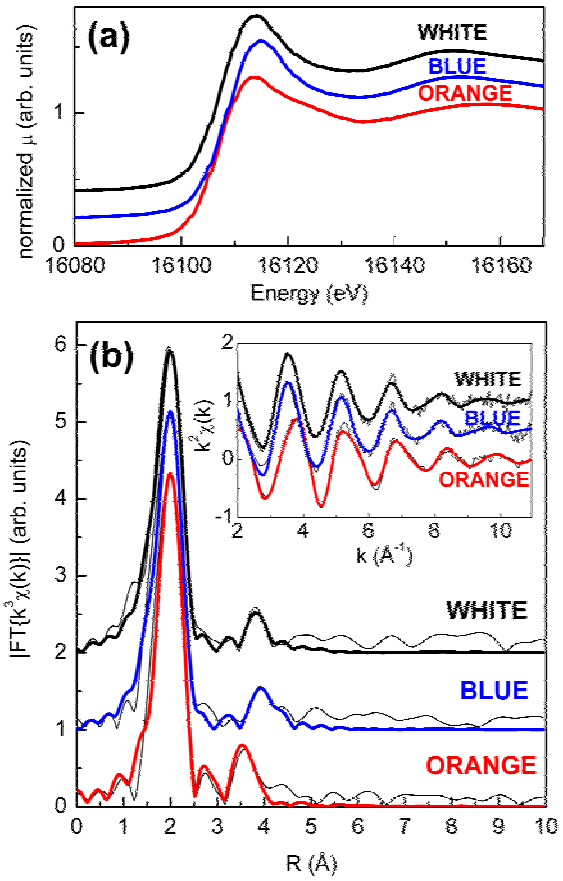

Figure 5: Sr K-edge XAFS spectra. *Representative Sr K-edge XAFS spectra recorded from the white, orange and blue regions:* ***(a)*** *The XANES spectra are vertically shifted for clarity.* ***(b)*** *Fitting of the EXAFS spectra in R- and k- (shown in the inset) space. The experimental spectra and the fitting curves are plotted in thin and thick solid lines, respectively*

Table II: Fitting results of the Sr-K-edge EXAFS spectra*. T, N, R and σ^2 stand for the type of the neighbouring atom, the nearest neighbor distance and the Debye-Waller factor. The quoted errors are uncertainties are provided by the FEFFIT program. The bonding configuration of Ca in calcite and aragonite ($CaCO_3$) and Sr in strontianite ($SrCO_3$) model compounds is also listed for comparison. In aragonite and strontianite average values for R and N are given in parenthesis for close-lying shells.*

Shell	**T**	**N**	**R (Å)**	**σ^2 (Å^2)**
Orange region				
1	O	6	2.53 ± 0.01	0.010 ± 0.001
2	C	6	3.35 ± 0.04	0.031 ± 0.009
3	O	6	3.67 ± 0.03	0.025 ± 0.006
4	Ca	6	4.10 ± 0.03	0.024 ± 0.003
White region				
1	O	9	2.61 ± 0.01	0.015 ± 0.001
2	C	8	3.00 ± 0.02	0.033 ± 0.002
3	Ca	6	4.20 ± 0.02	0.022 ± 0.003
4	O	13	4.34 ± 0.03	0.027 ± 0.004
5	Ca	4	4.52 ± 0.03	0.025 ± 0.006
Blue region				
1	O	9	2.60 ± 0.01	0.014 ± 0.001
2	C	8	3.00 ± 0.02	0.037 ± 0.004
3	Ca	6	4.24 ± 0.02	0.026 ± 0.004
4	O	13	4.35 ± 0.03	0.035 ± 0.006
5	Ca	4	4.56 ± 0.03	0.017 ± 0.006
Model compounds				
Shell	**T**	**N**	**R (Å)**	
Calcite, R-3c, a=b=4.99 Å, c=17.06 Å α=β=90º, γ=120º *				
1	O	6	2.36	
2	C	6	3.21	
3	O	6	3.46	
4	Ca	6	4.04	
Aragonite, Pmcn, a=4.9614 Å, b=7.9671 Å, c=5.7404 Å, α=β=γ=90º **				
1	O	1,2,2,2,2 (9)	2.42, 2.44, 2.52, 2.55, 2.65 (2.53)	
2	C	1,2,1,2 (6)	2.90, 2.94, 3.25, 3.41 (3.14)	
3	Ca	2,2,2 (6)	3.89, 3.95, 4.11 (3.98)	
4	O	1,2,1,2,2,3,2 (13)	3.92, 3.94, 4.01, 4.11, 4.12, 4.13, 4.17 (4.07)	
5	Ca	4	4.69	
Strontianite, Pmcn, a=5.090 Å, b=8.358 Å, c=5.997 Å, α=β=γ=90º **				
1	O	1,2,2,2,2 (9)	2.56, 2.58, 2.64, 2.65, 2.73 (2.64)	
2	C	1,2,1,2 (6)	3.03, 3.06, 3.41, 3.51 (3.26)	
3	Sr	2,2,2 (6)	4.10, 4.11, 4.26 (4.16)	
4	O	2,1,2,3,2,1,2 (13)	4.12, 4.14,4.24, 4.26, 4.28, 4.30, 4.36 (4.25)	
5	Sr	4	4.90	

*****Graf, 1961; ** de Villiers, 1971

4. Discussion

4.1. Colour variations along the claw

The colour variations observed macroscopically along the claw of *Callinectes sapidus* have an imprint on both the visible light reflectance and the Raman spectra. They are attributed to the presence of chromoproteins and the alterations induced in AXT. The reflectance spectra shown in Fig. 1(b) are in agreement with the spectra recorded previously from claws of female and male *C. sapidus* claws (Baldwin and Johnsen, 2012) and exhibit strong similarities with the reflectance spectra of red-orange and purple feathers obtained from different bird species (Mendes-Pinto *et al.*, 2012). In the case of birds, the characteristic colour has been attributed to the canthaxanthin carotenoid (van Wikj, 2005a) and its different binding in the feather chromoproteins. The reflectance spectra shown in Fig. 1(b) reveal that the orange part of the claw is associated with strong absorption in the green to violet spectral region (400 – 550 nm), whereas the blue part absorbs in the red to green (500 – 700 nm) spectral region. According to previous works (Begum *et al.*, 2015; Britton *et al.*, 1997; Buchwald and Jencks, 1968; Christensson *et al.*, 2013; Cianci *et al.*, 2002; Durbeej and Eriksson, *2003*; Goodwin, 1980; Ilagan *et al.*, 2005; Liu *et al.*, 2002; Salares *et al.*, 1977a, 1979; van Wikj, 2005a, 2005b; Weesie *et al.*, 1995;) related mainly to blue (crustacyanin) and yellow chromoproteins from lobsters, colour variations can be ascribed to a large number of possible mechanisms, like AXT aggregation, molecular exciton, enolate formation, interaction of the AXT molecules with the protein, planarization of the AXT molecule, charge transfer and polarization. Assuming that the chromoproteins in the crab are the same with those in lobsters, similar mechanisms should also be expected. However, even in this case, the question whether the same protein and its varying interactions with the carotenoid are responsible for the colour variation, or different proteins are involved in different stained regions, is still open. At this point the finding of Buchwald and Jencks (1968) for lobster should be invoked, where the yellow shell pigment (the absorption maximum shifts from 490 to 409 nm of the unbound AXT to that trapped in the chromoprotein) is a protein with molecular weight that differs from that of both the α- and the β- crustacyanins responsible for the colour of blue lobster. Furthermore, they reported that the amino acid content is also different, with the weight percentage of the aromatic amino acids being *ca.* 40% less compared to the case of crustacyanins. However, it should be mentioned that in another study (Zagalsky, 1982), the yellow proteins of the lobster carapace were reported to contain subunits both common and different to those that comprise the crustacyanins. Moreover in these proteins polydisperse behaviour in the number of AXT molecules per protein subunit has been observed.

4.2. Br preference for the stained parts of the claw

The XRF spectra revealed that Br is present in the orange and the blue regions of the claw, i.e. the same parts where the AXT is detected by Raman spectroscopy, revealing the co-localization of Br with the chromoprotein. The Br *K*-edge XANES spectra recorded in the orange and blue regions of the crab claw are very similar to the spectra of 4-Br-phenylalanine and 3,5-dibromotyrosine (Feiters *et al.,* 2005a). The corresponding Fourier transforms of the EXAFS spectra exhibit also strong similarities and show a very large contribution up to approximately 6 Å due to multiple scattering in the benzene ring. The EXAFS analysis results are in excellent agreement with the findings of Feiters *et al.* (2005a, 2005b) for these reference compounds, providing thus evidence for Br atoms being trapped in the phenyl and/or phenol rings located in the amino acid residues of the

chromophore protein. More specifically, 12 phenylalanine, 14 tyrosine and 2 tryptophan aromatic amino acid residues were reported in various crustacyanin proteins (1GKA, 1I4U, 1S44) in the protein data bank (Berman *et al.*, 2000; Cianci *et al.*, 2002; Gordon *et al.*, 2001; Habash *et al.*, 2004). Incorporation of Br in native bromoperoxidase enzyme from *Ascophyllum nodosum* by covalent bonding of Br to phenol rings of tyrosine residues has been verified by EXAFS (Feiters *et al.*, 2005). The nearest neighbour distances of Br detected in the stained parts of the claw are in agreement with the bromoperoxidase enzyme (Feiters *et al.*, 2005b), *p*-dibromobenzene (Schultz *et al.*, 1988), and in bromophenol pollutants (Bergknut *et al.*, 2008). It should be pointed out that the current study reveals a different phase than that described by Schofield *et al.* (2009). More specifically, in the case of the tips with the characteristic red staining of the claws of the crab *P. crassipes*, Br participates in the formation of a translucent separate phase with higher resistance to fracture compared to the calcified tissue. In the case of *C. sapidus* studied here, the whole claw is calcified, since Sr is detected thought the claw and participates in the $CaCO_3$ phases. On the contrary, Br is detected only in orange and blue stained parts of the claw. Staining exists in a surface layer of the outer part of the calcified exoskeleton. In a study on the jaws of the *Nereis* marine polychaete worm (Birkedal *et al.*, 2006), Br was also found to accumulate on the external surface of jaws. However, as in the case of Br-rich uncalcified tissue of *P. crassipes* (Schofield *et al.*, 2009), in the stained part of the claw of *C. sapidus* studied here, Br was found to be bound to phenyl and/or phenol rings which are present in the chromophore proteins responsible for the orange or blue staining. It is not incorporated either in the inorganic ($CaCO_3$ mineral) or the organic (chitin) part of the cuticle and it is not bonded to the end, ionone, rings of the AXT chromophore. The C-C bonds which are present in the AXT rings are not of the same length and differ considerably from those determined in the current study. Furthermore, the AXT rings are not perfectly planar leading up to less pronounced multiple scattering. Binding of Br in the polyene chain of AXT was also investigated but it provided much worse quality fitting, compared to Br bonded in the phenyl/phenol rings.

4.3. Biomineral differentiation at the claw fingers

Sr is found to substitute for Ca and functions as a probe of the type of formed biomineral, thus offering the advantage of measuring XAFS spectra at the Sr *K*-edge rather than at the lower energy Ca *K*-edge (Tester *et al.*, 2013). $CaCO_3$ is stabilized in different phases along various parts of the claw. More specifically, in the claw fingers calcite is dominant whereas in the palm an aragonite-like phase dominates. These variations were verified by both XAFS and Raman spectroscopy. Substitution of Ca by Sr was also observed in earthworm-secreted calcium carbonate granules produced in Sr containing soil, where calcite was the dominant phase (Brinza *et al.*, 2013). In the same work, the substitution of Ca by Sr in vaterite was also reported. The Sr-O distance was found equal to 2.51 and 2.55 Å in Sr adsorbed onto calcite and Sr co-precipitated with vaterite, respectively. Substitution of the Ca atoms by the larger Sr atoms in calcite resulted in an increase of the Sr-O distance by +7.2%. The nearest neighbour distances (Sr-O, Sr-C and Sr-Ca) reported for calcite (Brinza *et al.* 2013; Tester *et al.*, 2013) are in agreement with the corresponding distances detected in the spectrum from the orange part of the claw. Additionally, the distances detected in the blue and white part of the claw (palm) are in agreement with those reported for aragonite in fish otoliths (Doubleday *et al.*, 2013). Finch and Allison (2007) studied the bonding environment of Sr in calcite and aragonite where they found that Sr substitutes for Ca causing 6.5% and 2% dilation of the site, respectively, with the corresponding Sr-O distances being 2.51 and 2.58 Å. These values

are very close to the values obtained here for the fingers and the palm of the crab claw, respectively. They have also shown that the Sr *K*-edge XANES spectra are fingerprints of the Sr-containing calcite and aragonite. The Sr *K*-edge XANES spectra presented here from the blue and the white parts of the claw are similar to the spectra of strontianite and Sr-containing aragonite and vaterite (Brinza *et al.*, 2013; Finch and Allison, 2007). On the contrary, the spectrum recorded from the orange part of the claw resembles the spectrum reported for poorly crystallized calcite (Tester *et al.*, 2013).

The calcite and aragonite phases detected in the fingers and the palm of the claw should be termed as nano-crystalline, since short-range order is observed in the EXAFS spectra although with considerable static disorder that is evident from the high values of the Debye-Waller factors. Such a distortion of the $CaCO_3$ nanocrystals is attributed to their small size and the fact that they are embedded in an organic matrix (Hild *et al.*, 2008). The formation of pure, well-crystallized $CaCO_3$ phases can be also excluded due to the high values of the FWHM of the ν_1 (CO_3) peak in the Raman spectra (Wehrmeister *et al.*, 2011). However, the slightly lower values of the FWHM of the peak at a tooth and the fingertip of the claw could be attributed to a better crystallized calcite phase most probably imposed by the necessity for a harder material at these positions. The splitting of the ν_1 (CO_3) vibrational mode in two broad peaks observed in the spectra recorded in the palm of the claw could be attributed to the coexistence of an amorphous and a nano-crystalline aragonite phase. Slight variations in the crystallinity index were observed at various spots of the palm. Amorphous-like calcite (6-fold coordination) could clearly result in shorter Sr-O distances (Tester *et al.*, 2013) than those observed in the palm of the claw. Amorphous phases, although metastable, are either stabilized by the organism for its entire life or act as precursors for the stabilization of crystalline phases (Levi-Kalisman *et al.*, 2002). ACC phases were detected in a number of cases. B. Hasse *et al.* (2000) studied the mineralized shell of the *Biomphalaria glabrata* snail: XRD measurements revealed that aragonite was the dominant calcium carbonate phase in the shell of adult snails whereas ACC was the main component of eggs. However, Ca *K*-edge EXAFS measurements revealed that even in the cases of XRD-amorphous samples, the calcium adopted an aragonite-like short range order. Well-defined EXAFS signal, due to the nearest neighbouring oxygen atoms, but with considerably increased structural disorder beyond 3 Å, was also reported in sternal deposits of the *Porceliio scaber* crustaceous before changing the cuticle (Becker *et al.*, 2003). Coexistence of ACC and calcite polymorphs was also detected in spicules formed by the ascidian *Pyura pachydermatina* (Aizenberg *et al.*, 2002) whereas coexistence of ACC and aragonite has been reported in larval shells (Weiss *et al.*, 2002). It is proposed that the phosphates detected in the Raman spectra throughout the claw, play an important role in the stabilization of the various $CaCO_3$ biominerals (Levi-Kalisman *et al.*, 2002) and especially their amorphous – like phases (Taylor *et al.*, 1993). The presence of phosphates in the exoskeleton of the *H. Americanus* lobster and the *C. pagurus* crab has been reported (Boßelmann *et al.*, 2007). The observed variation in the $CaCO_3$ biominelarization in the claw fingers could be imposed from the necessity for different mechanical properties along the claws. For example, crabs use their claws to hold and crack prey or to burrow holes and therefore it is expected that they should have better mechanical properties compared to other parts of the cuticle (Seed and Hughes, 1995; Zhou *et al*., 2010) adopting for that reason different structures.

5. Conclusions

XAFS and Raman spectroscopies were applied for the study of the colour variations and the bonding configuration of Br and Sr along the claw of the *Callinectes sapidus* crab. The visible light reflectivity spectra are affected by the shifts in the absorption maximum of the astaxanthin carotenoid that is bonded to the blue or orange chromophore protein. The Br co-localization with the chromophore protein is verified by the combination of the Raman and XRF spectra. Furthermore, Br is bonded to phenyl and/or phenol rings most probably of amino acid residues of the chromophore protein. Combined Sr *K*-edge XAFS and Raman analysis revealed bio - mineralization variations along the claw. Sr was found to substitute for Ca in the $CaCO_3$ phase causing the expected lattice dilation due to its larger atomic volume. A small contribution of phosphate was also detected by Raman. Nano-crystalline calcite and aragonite phases were found to prevail in the finger and palm of the claw, respectively. In the latter case, the presence of an amorphous - like calcium carbonate phase that resembles the aragonite structure in the most proximal neighbouring shell is found to coexist with the nano-crystalline one. The variations in the biomileralization in fingers of the claw are attributed to the necessity for improved mechanical properties at its end.

Acknowledgements
The measurements at HASYLAB-DESY were funded from the European Community's Seventh Framework Programme (FP7/2007-2013) under grant agreement n° 312284. The support of Dr. Roman Chernikov during the beamtime at HASYLAB is greatly acknowledged.

References

Addadi, L., Joester, D., Nudelman, F., Weiner, S., 2006. Mollusk shell formation: A source of new concepts for understanding biomineralization processes. Chem. Eur. J. 12, 980–987.

Aizenberg, J., Lambert, G., Addadi, L., Weiner, S., 1996. Stabilization of amorphous calcium carbonate by specialized macromolecules in biological and synthetic precipitates. Adv. Mater. 8, 222–226.

Aizenberg, J., Lambert, G., Weiner, S., Addadi, L., 2002. Factors involved in the formation of amorphous and crystalline calcium carbonate: A study of an ascidian skeleton. J. Am. Chem. Soc. 124, 32–39.

Baldwin, J., Johnsen, S., 2012. The male blue crab, *Callinectes sapidus*, uses both chromatic and achromatic cues during mate choice. J. Exper. Biol. 215, 1184–1191.

Becker, A., Bismayer, U., Epple, M., Fabritius, H., Hasse, B., 2003. J. Shi, and A. Ziegler. Structural characterisation of X-ray amorphous calcium carbonate (ACC) in sternal deposits of the crustacea *Porcellio scaber.* Dalton Trans. 551–555.

Begum, S., Cianci, M., Durbeej, B., Falklöf, O., Hädener, A., Helliwell, J.R., Helliwell, M., Regan, A.C., Watt, C.I.F., 2015. On the origin and variation of colors in lobster carapace. Phys. Chem. Chem. Phys. 17, 16649–17502.

Behrens, G., Kuhn, L.T., Ubic, R., Heuer, A.H., 1995. Raman spectra of vateritic calcium Carbonate. Spectrosc. Lett. 28, 983–995.

Bergknut, M., Persson, P., Skyllberg, U., 2008. Molecular characterization of brominated persistent pollutants using extended X-ray absorption fine structure (EXAFS) spectroscopy. Anal. Bioanal. Chem., 390, 921–928.

Berman, H.M., Westbrook, J., Feng, Z., Gilliland, G., Bhat, T.N., Weissig, H., Shindyalov, I.N., Bourne, P.E., 2000. The Protein Data Bank. Nucleic Acids Res. 28, 235-242; www.rcsb.org

Bigi, A., Boanini, E., Capuccini, C., Gazzano, M., 2007. Strontium-substituted hydroxyapatite nanocrystals. Inorg Chim Acta 360,1009–1016.

Birkedal, H., Khan, R.K., Slack, N., Broomell, C., Lichtenegger, H.C., Zok, F., Stucky, G.D., Waite, J.H., 2006. Halogenated veneers: protein cross-linking and halogenation in the jaws of *Nereis*, a marine polychaete worm. ChemBioChem 7, 1392–1399.

Booth, C. H., Bridges, F, 2005. Improved self-absorption correction for fluorescence measurements of extended x-ray absorption fine-structure. Physica Scripta T115, 202–204.

Boßelmann, F., Romano, P., Fabritius, H., Raabe, D., Epple, M., 2007. The composition of the exoskeleton of two crustacea: The American lobster *Homarus americanus* and the edible crab *Cancer pagurus*. Thermochim. Acta 463, 65–68.

Brinza, L., Quinn, P.D., Schofield, P.F., Mosselmans, J.F.W., Hodson, M.E., 2013. Incorporation of strontium in earthworm-secreted calcium carbonate granules produced in strontium-amended and strontium-bearing soil. Geochim. Cosmochim. *Ac.* 113, 21–37.

Britton, G., Weesie, R.J., Askin, D., Warburton, J.D., Gallardo-Guerrero, L., Jansen, F.J., de Groot, H.J.M., Lugtenburg, J., Cornard, J.-P., Merlin, J.-C., 1997. Carotenoid blues: Structural studies on Carotenoproteins. Pure Appl. Chem. 69, 2075–2084.

Buchwald M., Jencks, W.P., 1968. Properties of the crustacyanins and the yellow lobster shell pigment, Biochem. 7, 844–859.

Cartwright, J.H.E., Checa, A.G., Gale, J.D., Gebauer, D., Sainz-Diaz, C.I., 2012. Calcium Carbonate Polyamorphism and Its Role in Biomineralization: How Many Amorphous Calcium Carbonates Are There? Angew. Chem. Int. Ed. 51, 11960–11970.

Cianci, M., Rizkallah, P.J., Olczak, A., Raftery, J., Chayen, N.E., Zagalsky, P.F., Helliwell, J.R., 2002. The molecular basis of the coloration mechanism in lobster shell: β-Crustacyanin at 3.2-Å resolution. Proc. Nat. Acad. Sci. 99, 9795–9800; www.rcsb.org, PDB ID: 1GKA.

Christensson, N., Žídek, K., Magdaong, N.C.M., La Fountain, A.M., Frank, H.A., Zigmantas, D., 2013. Origin of the Bathochromic Shift of Astaxanthin in Lobster Protein: 2D Electronic Spectroscopy Investigation of β-Crustacyanin. J. Phys. Chem. B 117, 11209–11219.

Chung, H.Y., Joyce Ma, W.C., Kim, J.-Shin, 2003. Seasonal distribution of bromophenols in selected Hong Kong seafood. J. Agr. Food Chem. 51, 6752–6760.

de Villiers, J.P.R., 1971. Crystal structures of aragonite, strontianite, and witherite. Am. Mineral. 56 758–767.

Doubleday, Z. A., Harris, H. H., Izzo, C., Gillanders, B. M., 2014. Strontium Randomly Substituting for Calcium in Fish Otolith Aragonite. Anal. Chem. 86, 865–869.

Durbeej, B., Eriksson, L.A., 2003. On the bathochromic shift of the absorption by astaxanthin in crustacyanin: a quantum chemical study. Chem. Phys. Lett. 375, 30 – 38.

Ermakov, I.V., Sharifzadeh, M., Bernstein, P.S., Gellermann, W., 2010 in: Landrum, J.T. (Ed.), Application of resonance Raman spectroscopy to the detection of carotenoids in vivo, in Carotenoids: Physical, Chemical, and Biological Functions and Properties, CRC Press (Taylor and Francis Group), Boca Raton, 2010.

Feiters, M.C., Küpper, F.C., Meyer-Klaucke, W., 2005a. X-ray absorption spectroscopic studies on model compounds for biological iodine and bromine. J. Synchrotron Rad. 12, 85–93.

Feiters, M.C., Leblanc, C., Küpper, F.C., Meyer-Klaucke, W., Michel, G., Potin, P., 2005b. Bromine is an endogenous component of a vanadium bromoperoxidase. J. Am. Chem. Soc. 127, 15340 – 15341.

Finch, A.A., Allison, N., 2007. Coordination of Sr and Mg in calcite and aragonite. Mineral. Mag. 71, 539–552.

Foster, L. C., Allison, N., Finch, A. A., Andersson, C., 2009. Strontium distribution in the shell of the aragonite bivalve *Arctica islandica*. Geophys. Geosyst. 10, Q03003.

Gibbs, P.E., Bryan, G.W., 1972. A study of strontium, magnesium, and calcium in the environment and exoskeleton of decapod crustaceans, with special reference to *Uca burgersi* on Barbuda, West Indies. J. Exp. Mar. Biol. Ecol. 9, 97–110.

Gong, Y.U.T., Killian, C.E., Olson, I.C., Appathurai, N.P., Amasino, A.L., Martin, M.C., Holt, L.J., Wilt, F.H., Gilbert, P.U.P.A., 2012. Phase transitions in biogenic amorphous calcium carbonate. Proc. Natl. Acad. Sci. 109, 6088–6093.

Gordon, E.J., Leonard, G.A., McSweeney, S., Zagalsky, P.F., 2001. The C1 subunit of alpha-crustacyanin: the de novo phasing of the crystal structure of a 40 kDa homodimeric protein using the anomalous scattering from S atoms combined with direct methods. Acta Crystallogr. D57, 1230–1237; www.rcsb.org, PDB ID: 1I4U.

Goodwin, T.W., 1980. The Biochemistry of the Carotenoids: Volume II Animals. Chapman and Hall.

Habash, J., Helliwell, J.R., Raftery, J., Cianci, M., Rizkallah, P.J., Chayen, N.E., Nneji, G.A., Zagalsky, P.F., 2004. The structure and refinement of apocrustacyanin C2 to 1.3 Å resolution and the search for differences between this protein and the homologous apoproteins A1 and C1. Acta Crystallogr. D60, 493–498; www.rcsb.org, PDB ID:1S44.

Hadley, N.F., 1986. The Arthropod Cuticle. Sci. Am. 7, 98-106.

Hasse, B., Ehrenberg, H., Marxen, J.C., Becker, W., Epple, M., 2000. Calcium carbonate modifications in the mineralized shell of the freshwater snail *Biomphalaria glabrata*. Chem. Eur. J. 6, 3679–3685.

Hild, S., Marti, O., Ziegler, A., 2008. Spatial distribution of calcite and amorphous calcium carbonate in the cuticle of the terrestrial crustaceans *Porcellio scaber* and *Armadillidium vulgare*. J. Struct. Biol. 163, 100–108.

Ilagan, R.P., Christensen, R.L., Chapp, T.W., Gibson, G.N., Pascher, T., Polívka, T., Frank, H.A., 2005. Femtosecond time-resolved absorption spectroscopy of astaxanthin in solution and in α-crustacyanin. J. Phys. Chem. A 109, 3120–3127.

Janssens, K.H.A., Adams, F.C.V., Rindby A. (Eds.), 2000. Microscopic X-Ray Fluorescence Analysis, Wiley, Chichester.

Kaczor, A., Baranska, M., 2011. Structural changes of carotenoid astaxanthin in a single algal cell monitored *in situ* by Raman spectroscopy. Anal. Chem. 83, 7763–7770.

Katsikini, M., Mavromati, A., Pinakidou, F., Paloura, E.C., Gioulekas, D., Ioannides, D., Erko, A., Zizak, I., 2010. Application of conventional and microbeam synchrotron radiation X-ray fluorescence and absorption for the characterization of human nails. J. Nanosci. Nanotechnol. 10, 6266–6275.

Lavalli, K.L., Spanier, E., 2007. The Biology and Fisheries of the Slipper Lobster. Taylor and Francis Group, 2007, p. 185.

Levi-Kalisman, Y., Raz, S., Weiner, S., Addadi, L., Sagi, I., 2002. Structural differences between biogenic amorphous calcium carbonate phases using X-ray absorption spectroscopy. Adv. Funct. Mater. 12, 43–48.

Liu, J., Shelton, N.L., Liu, R.S.H., 2002. Study of α-crustacyanin utilizing halogenated canthaxanthins. Org. Lett. 4, 2521–2524.

Marxen, J.C., Becker, W., Finke, C., Hasse, B., Epple, M., 2003. Early mineralization in *Biomphalaria glabrata*: Microscopic and structural results. J. Moll. Stud. 69, 113–121.

Mendes-Pinto, M.M., La Fountain, A.M., Caswell Stoddard, M., Prum, R.O., Frank, H.A., Robert, B., 2012. Variation in carotenoid–protein interaction in bird feathers produces novel plumage coloration. J. R. Soc. Interface 9, 3338–3350.

Nagasawa, H., 2012. The crustacean cuticle: Structure, composition and mineralization. Front. Biosci. (Elite Ed) 4, 711–720.

Newville, M., Ravel, B., Haskel, D., Rehr, J.J., Stern, E.A., Yacoby, Y., 1995. Analysis of multiple scattering XAFS data using theoretical standards. Physica B 208, 154–156.

Penel, G., Leroy, G., Rey, C., Bres, E., 1998. Micro-Raman Spectral Study of the PO_4 and CO_3 vibrational modes in synthetic and biological apatites. Calcif. Tissue Int. 63, 475–481.

Poiarkova A. V., Rehr J. J., 1999. Multiple-scattering x-ray-absorption fine-structure Debye-Waller factor calculations. Phys. Rev. B 59, 948–957.

Ravel, B., Newville, M., 2005. ATHENA, ARTEMIS, HEPHAESTUS: Data analysis for X-ray absorption spectroscopy using IFEFFIT. J. Synchr. Radiat. 12, 537–541.

Raz, S., Weiner, S., Addadi, L., 2000. Formation of high-magnesian calcites *via* an amorphous precursor phase: possible biological implications. Adv. Mater. 12, 38–42.

Rehr, J.J., Albers, R.C., 2000. Theoretical approaches to X-ray absorption fine structure. Rev. Mod. Phys. 72, 621–654.

Rez, P., Sinha, S., Gal, A., 2014. Nanocrystallite model for amorphous calcium carbonate. J. Appl. Cryst. 47, 1651–1657.

Rimai, L., Heyde, M.E., Gill, D., 1973. Vibrational spectra of some carotenoids and related linear polyenes. A Raman spectroscopic study. J. Am. Chem. Soc. 95, 4493–4501.

Salares, V.R., Young, N.N., Bernstein, H.J., Carey, P.R., 1977a. Resonance Raman spectra of lobster shell carotenoproteins and a model astaxanthin aggregate. A possible photobiological function for the yellow protein. Biochemistry 16, 4751–4756.

Salares, V.R., Young, N.M., Carey, P.R., Bernstein, H.J., 1977b. Excited state (excitation) interactions in polyene aggregates. Resonance Raman and absorption spectroscopic evidence. J. Raman Spectrosc. 6, 282–288.

Salares, V.R., Young, N.M., Bernstein, H.J., Carey, P.R., 1979. Mechanisms of spectral shifts in lobster carotenoproteins. The resonance Raman spectra of ovoverdin and the crustacyanins. Biochim. Biophys. Ac. 576 176–191.

Schofield, R.M.S., Niedbala, J.C., Nesson, M.H., Tao, Y., Shokes, J.E., Scott, R.A., Latimer, M.J., 2009. Br-rich tips of calcified crab claws are less hard but more fracture resistant: a comparison of biomineralized and heavy-element biomaterials. J. Struct. Biol. 166, 272–287.

Schultz, G., Kolonits, M., Hargittai, I., Portalone, G., Domenicano, A., 1988. Molecular structure and ring distortions of *p*-dibromobenzene as determined by electron diffraction. J. Mol. Struct. 176, 71–80.

Seed, R., Hughes, R.N., 1995. Criteria for prey size-selection in molluscivorous crabs with contrasting claw morphologies. J. Exp. Mar. Biol. Ecol. 193 177–195.

Siegel, F., 1960. The effect of strontium on the aragonite-calcite ratios of Pleistocene corals. J. Sedim. Res. 30, 297–304.

Sunagawa, I., Takahasji, Y., Kiroyuki, I., 2007. Strontium and aragonite-calcite precipitation. J. Mineral. Petrol. Sci. 102, 174–181.

Taft, W. H., 1967. Modern carbonate sediments ,in Chilingar, G. V., Bissell, H. J., Fairbridges, R. W. (Eds.) Carbonate Rocks: Origin, Occurrence and Classification. Elsevier, Amsterdam, pp. 35–40.

Taylor, M.G., Simkiss, K., Greaves, G.N., Okazaki, M., Mann, S., 1993. An X-ray absorption spectroscopy study of the structure and transformation of amorphous calcium carbonate from plant cystoliths. Proc. R. Soc. Lond. B 252, 75-80.

Tester, C.C., Wu, C.-H., Krejci, M.R., Mueller, L., Park, A., Lai, B., Chen, S., Sun, C., Balasubramanian, M., Joester, D., 2013. Time-resolved evolution of short- and long-range order during the transformation of amorphous calcium carbonate to calcite in the sea Urchin Embryo. Adv. Funct. Mater. 23, 4185–4194.

Tilley, R. J. D., 2011. Colour and the optical properties of materials, second ed., Wiley.

van Wikj, A., 2005a. The Color of Lobsters: The Bathochromic Shift of Astaxanthin in α-Crustacyanin, PhD Thesis, Universiteit Leiden.

van Wijk, A.A.C., Spaans, A., Uzunbajakava, N., Otto, C., de Groot, H.J.M., Lugtenburg, J., Buda, F., 2005b. Spectroscopy and quantum chemical modeling reveal a predominant contribution of excitonic interactions to the bathochromic shift in α-crustacyanin, the blue carotenoprotein in the carapace of the lobster *Homarus gammarus*. J. Am. Chem. Soc. 127, 1438-1445.

Weesie, R.J., Askin, D., Jansen, F.J.H.M., de Groot, H.J.M., Lugtenburg, J., Britton, G., 1995. Protein-chromophore interactions in α-crustacyanin, the major blue carotenoprotein from the carapace of the lobster, *Homarus gammarus:* A study by ^{13}C magic angle spinning NMR. FEBS Lett. 362, 34–38.

Weesie, R.J., Merlin, J.C., Lugtenburg, J., Britton, G., Jansen, F.J.H.M., Cornard, J.P., 1999. Semiempirical and Raman spectroscopic studied of carotenoids. Biospectroscopy 5, 19–33.

Wehrmeister, U., Jacob, D.E., Soldati, A.L., Loges, N., Häger, T., Hofmeister, W., 2011. Amorphous, nanocrystalline and crystalline calcium carbonates in biological materials. J. Raman Spectrosc. 42, 926 – 935.

Weiner, S., Levi-Kalisman, Y., Raz, S., Addadi, L., 2003. Biologically Formed Amorphous Calcium Carbonate. Connect. Tissue Res. 44, 214–218.

Weiss, I.M., Tuross, N., Addadi, L., Weiner, S., 2002. Mollusc larval shell formation: amorphous calcium carbonate is a precursor phase for Aragonite. J. Exp. Zool. 293, 478–491.

Wopenka, B., Pasteris, J., A mineralogical perspective on the apatite in bone, *Mater. Sci. Engin. C*, 25 (2005) 131-143.

Zagalsky, P.F., 1982. The study of the yellow astaxanthin-proteins of lobster carapace. Comp. Biochem. Physiol. 71B, 243–247.

Zhou, F., Wu, Z., Wang, M., Chen, K., 2010. Structure and mechanical properties of pincers of lobster (*Procambarus clarkii*) and crab (*Eriocheir Sinensis*). J. Mech. Behav. Biomed. 3, 454–46.

Zougrou, I. M., Katsikini, M., Pinakidou, F., Paloura, E. C., Papadopoulou, L., Tsoukala, E., 2014. Study of fossil bones by synchrotron radiation micro-spectroscopic techniques and scanning electron microscopy. J Synchrotron Radiat, 21, 149–160.